Polydispersity and Composition Stability in a Long-Term Follow-Up of Palmarosa (*Cymbopogon Martini*) and Tea Tree (*Melaleuca Alternifolia*) O/W Nanoemulsions for Antibacterial Use

Erick Sánchez-Gaitán [†] [ID], Vianney González-López [†] [ID] and Francisco Delgado *,[†] [ID]

Tecnologico de Monterrey, School of Engineering and Science, Atizapan 52926, Mexico; erickjsg@tec.mx (E.S.-G.); vianneyg@tec.mx (V.G.-L.)
* Correspondence: fdelgado@tec.mx
[†] These authors contributed equally to this work.

Abstract: There is a growing focus on the design of nanoemulsions because of their valuable properties as an enhanced vehicle for interaction with cells and resistant bacteria. Their potential applications in the health and food industry are numerous. Although they are considered unstable because of flocculation and coalescence, they are still efficient resources for antibacterial inhibition due to their droplet size. Studies on the interactions between essential oils and an aqueous medium are increasing, in order to efficiently formulate them at the nanometric scale using surfactants, thereby providing them with long-lived droplet size stability. This study used the ultrasonication method for fabrication and Eumulgin as a surfactant to achieve nanometric droplet sizes using two noble essential oils, palmarosa and tea tree. A follow-up for one year tracked a stable droplet size and sustained polydispersity in those emulsions as the most valuable outcome. Moreover, the insights of a thermoresponsive study have been included, also showing a strong stability. The antibacterial properties of the essential oils considered became enhanced, at a comparable scale of an antibiotic, on *Salmonella* spp. and *Bacillus subtilis* depending on the nanoscale droplet size. The outcomes suggest the importance of deepening parametric studies of these nanoformulations in terms of concentrations and temperature changes, characterizing their remarkable properties and durability.

Keywords: nanostructures; nanoemulsions; O/W emulsions; characterization; droplet size stability; kinetical stability; thermodynamic stability; interface efficiency; antibacterial properties

1. Introduction

Bacteria acquiring resistance to the most common antibiotics pose a risk to public health by increasing morbidity and mortality rates worldwide. To replace them, more aggressive medications or higher doses of drugs have been applied, leading to severe organ damage and long recovery times. Instead, the prophylactic use of essential oils in emulsions provides an alternative complementary safe solution [1–3]. The application of emulsions on the nanometric scale has increased significantly in areas such as the pharmaceutical [4], food [5], agricultural, cosmetic, and materials industries due to the potential advantages they offer compared to conventional emulsions [6].

Emulsions are colloidal dispersions composed of two immiscible substances that are notable for being stabilised at their interfaces by surfactants, reducing the interfacial tension

between them [7,8]. Those emulsions exhibit antibacterial features through the inclusion of nanosized droplets of certain essential oils (EOs), which improve the bioavailability of active compounds, inhibiting the growth of bacteria and fungi. Regarding characterisation, several authors have established a droplet size of 20 to 200 nm as characterising a nanoemulsion (NE) [9,10]. They are associated with several properties, such as transparency, increased bioavailability, and the solubility of hydrophobic compounds [6,7,9,11,12], but also with notable physicochemical stability, a rheological modification capacity, and dispersibility [13].

Oil in Water (O/W) emulsions have oil droplets dispersed in an aqueous medium [14]. A third immiscible interface, commonly added, is an emulsifier or surfactant that boosts stability by lowering interfacial tension. NEs are termed kinetically stable, as they have the capacity to prevent a limited spontaneous separation of the dispersed phase, but that does not imply thermodynamic stability, so they could still coalesce or flocculate over time [12,15,16]. Although thermodynamic stability is commonly achieved by microemulsions (MEs), there is no clear and unique difference between NEs and MEs in terms of their droplet size and fabrication methods [9,17].

There are different commonly classified methods used to obtain NE and ME, according to the energy applied to the initial emulsion [18]. Low-energy methods ($\approx 10^3$ W/kg) consist of mixing the emulsion components with external low-energy sources such as heat. In contrast, high-energy methods (such as ultrasound and high-pressure microfluidization) require energy rates around $\approx 10^{10}$ W/kg by using external sources to fragment the droplets, thus reducing their size. Ultrasound is the lowest energy-consuming method in the group of high-energy methods, as it also requires fewer emulsifiers to form small droplets on a nanoscale [19–21] and allows for greater control of their resulting size. They still ensure the preservation of several properties of the emulsions [10,22]. Commonly, low-energy methods are related to ME fabrication, practically as a spontaneous process, while high-energy methods are related to NE fabrication as induced methods. Today, this criterion prevails partially in the classification of NEs and MEs.

EOs are extracted from a diversity of plants using distillation and are widely used in many industries due to their beneficial properties and scents [23,24]. They comprise 20 to 60 bioactive compounds, but only two or three are found in higher concentrations and are responsible for these properties [25]. In particular, their microbial susceptibility has led to them being considered as a safer alternative for treating bacterial resistance in several works [25–31]. The EOs of *Cymbopogon martini* and *Melaleuca alternifolia* (known as palmarosa and tea tree oils, respectively) have been traditionally and contemporaneously identified for diverse applications in cosmetology [32], medicine [33], toxicology [34], food security, and health, with specific antifungal [27] and antibacterial [35] characteristics. These studies do not necessarily involve nanoscale applications. However, although some studies considered EOs in coarse emulsions, there are introductory studies suggesting the enhancement of their properties when the droplet size is on the nanoscale [36,37].

In practice, the previously mentioned EOs (palmarosa and tea tree) have been extensively considered due to their representative antimicrobial properties against microorganisms [25,38]. Geraniol and terpinen-4-ol are monoterpene compounds present therein, which exhibit antimicrobial properties due to their lipophilicity, permeabilizing cell membranes by binding to important intracellular sites and causing functional and structural damage [39]. By applying these compounds at the nanoscale, the permeability of the cell membrane increases [40,41]. Thus, nanoscale emulsions have been proposed as an alternative method against Gram-positive and Gram-negative bacterial pathogens [1].

Here, using ultrasonication, O/W emulsions based on palmarosa and tea tree oils have been nanofabricated as effective antibacterial agents. They were not fabricated spon-

taneously using low-energy methods but through an induced ultrasound process, thereby falling into the NE criterion. They are representative candidates for nanoscale emulsions because of their antimicrobial effects and affordability. We investigated their chemical composition through spectroscopic analysis after ultrasonication to ensure the presence of antimicrobial compounds. One of the main outcomes of this research is the stability of long-lived droplets size tracked over one year after droplet size distributions and their dynamics, monitored using dynamic light scattering (DLS) to show stable droplets at the nanoscale (1–100 nm). The incursion into the thermoresponsive effects also opens up further studies around the droplet size-based transport dynamics. Disk diffusion studies determined certain enhanced inhibitory activity against exemplary Gram-positive and Gram-negative bacteria, showing them as potential antibacterial agents, leading to future applications as an effective, accessible, and safe antiseptic product for commercial purposes. Section 2 presents the Materials and Methods. The third section presents the main results of the research. The two last sections comprise the discussion and conclusions.

2. Materials and Methods

2.1. Materials

2.1.1. Essential Oils, Surfactant, and Continuous Phase

Palmarosa and tea tree EOs were purchased from a local supplier (Droguería Cosmopolita, Mexico City, Mexico), with CAS (Chemical Abstracts Service) 8014–19–5 for palmarosa and CAS 6847-73-4 for tea tree. Both essential oils were pure (derived from a genuine botanical source without fillers, additives, or other impurities).

Eumulgin was chosen here as a surfactant because it is considered a safe substance for human use under a maximum daily exposure of 9 mg, according to the Food and Drug Administration (FDA) [42]. Hydrogenated castor oil of cosmetic grade Eumulgin CO 40 was purchased from a local supplier (Droguería Cosmopolita, Mexico City, Mexico) with CAS 61788-85-0. The continuous phase (distilled water) was acquired from CTR Scientific (Mexico City, Mexico), a national supplier of laboratory equipment and chemical reagents.

2.1.2. Bacterial Strains

To analyse the antibacterial characteristics of NEs, the bacterial strains considered were *Salmonella* spp. and *Bacillus subtilis*, representatives of Gram-negative and Gram-positive bacteria, respectively. They were acquired as clinical isolates obtained from the Autonomous University of Nuevo Leon (Monterrey, Mexico) and are commonly studied for their effect on the human body and their developed resistance to antibiotics. *Salmonella* spp. was selected due to its pathogenic activity and recent antibiotic resistance. *B. subtilis* was selected due to its versatility and its similarity in cellular structure to other Gram-positive pathogenic bacteria.

Becton Dickinson Bioxon nutrient, acquired from Master Leav (Puebla, Mexico), was used to promote bacterial growth for the disk diffusion test. Mueller–Hinton agar from Sigma-Aldrich Products, acquired from Master Leav (Puebla, Mexico), was used for the disk diffusion technique. Ampicillin from Sigma-Aldrich, acquired from CTR Scientific (Mexico City, Mexico), with a concentration of 100 mg/mL, was used to compare the effect of the emulsion. It is a broad-spectrum antibiotic that is effective against Gram-positive and Gram-negative bacteria. Filter paper disks with an approximate diameter of 6 mm were used to load the NE and antibiotic test.

2.2. Methods

The main research lines in this study (composition, droplet size, and disk diffusion) are briefly reported in Figure 1 ,together with the main analysis methods.
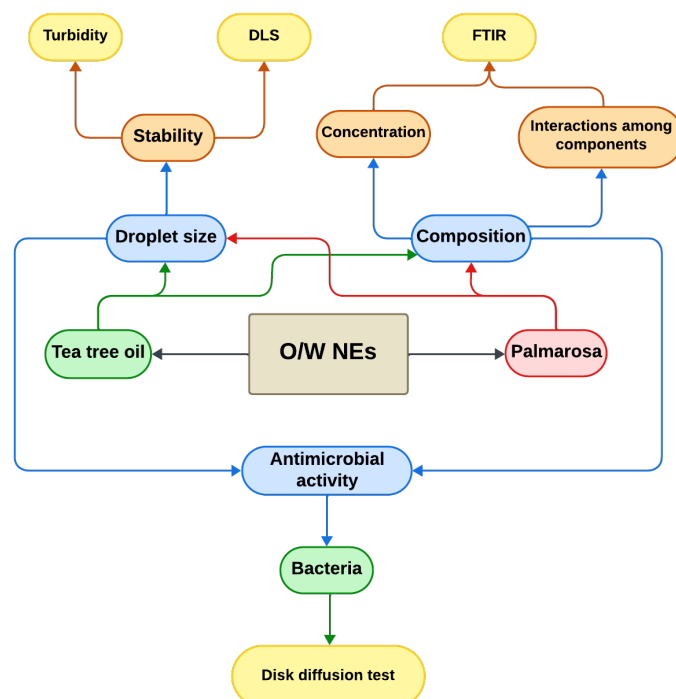
Figure 1. Distribution of the goals and results obtained for the tea tree and palmarosa emulsions in this study.

2.2.1. Microemulsion Preparation

Initial Preparation

The EO emulsions, at concentrations of 5% and 10% (w/w), were prepared by considering these proportions (w/w) of EOs, and then adding 13% and 21% (w/w) of Eumulgin or hydrogenated castor oil of Eumulgin, respectively, in a Corning tube measuring 20 mL. To reach those proportions, several previous studies were performed to obtain stable emulsions over time. Based on these results, we obtained a more homogeneous size distribution using 13% and 21% of Eumulgin, with droplets less than 15 nm. After the pre-mixture, distilled water was added to each solution, at 82% and 69% (w/w), respectively. Then, the mixtures were heated at a temperature of 45 °C for five minutes and mixed using Vortex-Genie 2 (Scientific Industries Inc., Hania, NY, USA), obtaining a milky white-coloured emulsion. After the initial preparation, but before ultrasonication, the droplet size of the emulsions was measured using DLS. The characteristic droplet size was around 900 nm. The results showed that nanoscale droplets (in the sense of the nanoemulsion characterisation criterion) did not appear as a spontaneous process. This measurement was repeated for several of days more with the same outcome. The size of the droplets was shown to be the result of the additional ultrasonication process rather than a spontaneous process.

Ultrasonication Method

The emulsions of palmarosa and tea tree were obtained using the ultrasonication method to form nanoscale droplets [43,44]. This resulted in kinetically stable NEs following the application of sound waves greater than 20 kHz. This method led to droplets with notable stability and droplet size at the nanoscale, which do not flocculate and coalesce over a long time and which control temperature changes.

After ultrasonication, a translucid colloid was obtained using a Hielscher UP4000St (Teltow, Germany) ultrasonic processor (400 W, 24 kHz). The emulsions were prepared for 1 min for 5% NE and for 1.5 min for 10% NE. An amplitude of 70% of the total power of the equipment was used and also 70% of the maximum frequency value. The emulsions were

placed in an ice bath to prevent overheating and the degradation of the EOs. Finally, they were transferred to test tubes with screw caps and stored in darkness at a non-controlled temperature of 20 °C, on average.

2.2.2. Composition Characterisation

In [45], DLS and Fourier transform infrared spectroscopy (FTIR) techniques were used to analyse the droplet size and composition of NEs. There, emulsions with different compositions exhibited extended droplet size distributions with various stability. Here, FTIR spectra were obtained using Shimadzu's IR Affinity-1S equipment (Kyoto, Japan) coupled with attenuated total reflectance (ATR). The emulsions and EOs (∼50 µL) were placed on the ATR. Similarly, 0.05 mg of Eumulgin was used to analyse their infrared absorption and elucidate their composition. The raw materials (Eumulgin, distilled water, and EOs) and the NEs were compared to observe certain functional groups and interactions between the components. The objective of acquiring the EOs from a local provider was to reduce the emulsion production costs without compromising their properties. The FTIR analysis ensured the adequate composition of both EOs.

2.2.3. Droplet Size Characterisation
Turbidity

Turbidity is a parameter influenced by several factors, including the type of essential oil, the composition of NEs, and the size of the droplets. Several studies have reported that the increase in turbidity is related to the interaction of light with larger particles in the NE, becoming a primary detection method [46,47]. Thus, an important property of NEs is their low turbidity, although samples at higher concentrations present a higher turbidity value. After the elaboration, the turbidity of the NEs was measured for each sample as a preliminary study to elucidate the size of droplets at the nanoscale. An HI887130-ISO Turbidimeter (acquired from HANNA Instruments, Mexico City, Mexico) was used to measure it.

Dynamic Light Scattering and Zeta Potential Measurement

As mentioned previously, in [45], the DLS technique was used to analyse the stability of the droplet size in nanoemulsions. In the current research, DLS was used to determine the polydispersity and droplet size of the emulsions using Zetasizer Advance Ultra equipment (DLS, Malvern Instruments, Worcestershire, UK). Those quantities were first determined just after their elaboration, followed by a tracking of the stability over time, as a result of efficient and effective nanofabrication. NEs were analysed using the backscattered method and a stabilising temperature of 25 °C. The emulsions were analysed by pouring approximately 1 mL into a low quartz cuvette. In addition to this equipment, a Folded Capillary Zeta Cell, DTS1070 (Malvern Instruments, Worcestershire, UK) was also used to determine the zeta potential of NEs.

Polydispersity

The polydispersity index (PDI) refers to the compositions of different sizes that form a sample. Typically, it provides information about the heterogeneity of droplet sizes. A low PDI value confirms the presence of a homogeneous distribution of droplet sizes. However, several measures exist for such an index. In the current analysis, we have reported and compared a couple of measures, designated here as PDI_a and PDI_b. PDI_a was determined, through the size datasets for the mean and standard deviation of the statistical distribution of the droplet size provided by the equipment, as $PDI_a = \sigma/\mu$. This measure is commonly associated with the Schulze–Hardy rule [48,49]. A lower PDI_a value suggests a more homogeneous distribution of sizes, while a higher value refers to

a heterogeneous distribution. Alternatively, PDI_b is the measure directly reported by the DLS instrument. It is derived from the moments of the logarithmic droplet size correlation function as $PDI_b = 2M_3/M_2^2$, with M_i as the ith moment [50,51]. It is closer to Kurtosis-like measures but is highly dependent on the measurement techniques used by each instrument. For the instrument used herein, a PDI_b value between 0.1 and 0.25 represents a narrow distribution [52], while values above 0.5 represent a broad distribution of droplet sizes [53].

2.2.4. Droplet Size Stability Follow-Up

The stability of the droplet size is a relevant parameter that helps to discriminate between kinetic and thermodynamic stability. When it changes, the emulsion may lose some of the properties potentiated by the nanoscale. There is controversy regarding droplet sizes between 10 and 100 nm and their definition as MEs or NEs, which does not correspond to their particular size but rather with their type of stability over time, polydispersity, and preparation method. The determination of thermodynamic stability is usually experimentally complex because its definition underlies the behaviour of the Gibbs free energy change with factors that modify the size of its droplets [54,55]. If this change $\Delta G = \sigma \Delta A - T \Delta S < 0$, then the increase in the interfacial area ΔA (the breakdown into droplets of smaller radius) occurs at the expense of an increase in entropy and is usually feasible for low interfacial tensions $\sigma \lessapprox 10^{-3}$–$10^{-1}$ mN/m [56]. This is dramatically different from the case of NEs, where $\sigma \approx 1$–10 mN/m and which can only achieve kinetic stability [57]. The stability of NEs has been a subject of discussion within the field.

To assess differences in the meaningful statistical changes of droplet size distributions, we used a mean difference test based on Student's t distribution. Even considering a low confidence for the difference in the mean diameter of the droplets, for example 80%, it will imply mean differences greater than approximately 1.282 times the standard deviation (considering an infinite number of degrees of freedom for large samples, as in this case). This would imply somewhat greater differences than the standard deviations involved in the distributions.

Stability of the Droplet Size Distribution

In our specific case, we used a high-energy method, corresponding with a criterion defining NEs, to obtain a kinetically stable droplet size [9,12,18]. Thus, while smaller droplets generate a larger total surface area, they could require more energy if the process is not spontaneously reached. For the follow-up, DLS tests were performed on each emulsion through different periods departing its fabrication (initial), then 1, 3, 6, and 12 months later. As an alternative test of stability, the zeta potential (ζ) of the emulsions was monitored at each time using the same DLS instrument, which provides this value by employing a zeta cell to measure it when transmitting an electric current through the emulsion. For this step, 1 mL of NE was taken by syringe and placed in the zeta cell to perform the measurement.

Insight Test of Thermoresponsiveness

However, several examples of long-lived NEs have been provided in the literature [58,59], some of which have a certain elastic thermoresponsivity [60–62]. Despite being outside the scope of the main objectives of this research, we developed an insight thermoresponsivity test based on DLS. In such a case, for 5% NEs, departing from a first measurement at room temperature, we raised the temperature to 50 °C by heating the sample (controlled by the DLS equipment). Then, a series of DLS measurements were performed, equally spaced, for 10 min each, until the visual equilibrium of the droplet size distribution plot was reached. The sample was then again cooled at room temperature, taking DLS measurements for the droplet size distribution with the same time lapses.

These measurements were also repeated until the visual equilibrium of the droplet size distribution plot was reached.

2.2.5. Antibacterial Activity

One of the main differences between Gram-negative and Gram-positive bacteria comes from their cell envelope. Gram-negative bacteria have an outer layer composed of lipopolysaccharides and an inner thin cell wall made of peptidoglycan. In contrast, Gram-positive bacteria only have a peptidoglycan cell wall, but these are many times thicker than those observed in Gram-negative bacteria [63].

In [64], the disk diffusion technique was applied to determine the efficacy of clove–thyme NEs on *Escherichia coli*, *Bacillus subtilis*, *Staphylococcus aureus*, and *Klebsiella oxytoca*. It showed a higher inhibitory effect of NEs than of coarse emulsions using the same EOs. Therefore, in this study, the disk diffusion method was applied to assess the antimicrobial activity of emulsions over representative Gram-positive and Gram-negative bacteria. Here, the oldest NE samples presented in the current work were used to show their sustained effectiveness through time.

The bacteria strains, *Salmonella* spp. and *Bacillus subtilis*, were placed in the nutrient broth for more than 15 h before inoculation. At that time, the optical density of *Salmonella* spp. corresponded to 1.369 and the optical density for *Bacillus subtilis* was 0.978, when both bacteria were in their logarithmic phase. Each agar plate was labelled and then inoculated before placing the inhibition disks. The emulsion and the antibiotic ampicillin were loaded onto a filter paper disk $d_b \sim 6$ mm in diameter. Each paper disk was loaded with 10 µL of the emulsions and the controls were placed at an approximate separation distance of 2 cm between each other on the surface of the inoculated agar. After 24 h of incubation at 37 °C, the diameter of the inhibition zone was determined for the emulsions and their controls. The measurement was made with Vernier callipers and was measured four times to reduce errors, ensuring accurate measurement of the inhibition disks and the diameter of the original paper disks. Each agar plate had a different emulsion and was analysed twice (repetitions labelled 1 and 2) to obtain better control of the experiment. Two additional dilutions of 50% and 25% (v/v) were used to determine antibacterial activity in lower concentrations of the original emulsion. The dilutions were obtained departing from the original NE; 1 mL of it was placed in 1 mL or 3 mL of distilled water inside a sterile tube using a micropipette, manually homogenising for 10 s to prepare the 50% or 25% (v/v) dilutions, respectively.

2.2.6. Summary

In summary (Figure 1), the composition of the emulsions and their respective raw materials was studied using FTIR coupled with ATR. Then, a study of the turbidity suggested the presence of nanoscale oil droplets in NE. For droplet size studies, repeated DLS measurements determined the change in droplet size over time. A brief thermoresponsive analysis was performed to obtain information about the droplets' stability strength. Finally, the effect of the droplet size and composition of the emulsions on microbial strains was studied using the disk diffusion method, compared with that of an effective antibiotic.

3. Results

3.1. Initial Characterisation

3.1.1. Turbidity Outcomes for the Fabricated NEs

The initial turbidity characterisation for the palmarosa NE with an EO concentration of 5% was 34.6 NTU (Nephelometric Turbidity Units), while, for 10% NE, it was 53.5 NTU. The tea tree NE with an EO concentration of 5% showed a turbidity of 33.8 NTU and, for a

10% NE, a turbidity of 50.6 NTU. Typically, turbidity values for similar oil concentrations in a typical microscale droplet emulsion fall between 100 and 500 NTU [65]. Instead, values near 30 NTU denote low turbidity, while those near 50 NTU correspond to low–moderate turbidity, as those obtained in our NE suggest droplet sizes far below 1 μm, closer to nanoscale droplets. As a reference, similar results were obtained for lecithin microemulsions [66] showing sizes of 4.4 to 6.3 nm, resulting in turbidity values between 11.53 and 13 NTU.

3.1.2. Composition Study After Ultrasonication

Figure 2A,B show the composition outcomes for palmarosa and tea tree emulsions using FTIR, one year after fabrication, to track their main antibacterial compounds. They are identical to those obtained just after their fabrication (a similar analysis of additional 10% emulsions in this study gave similar FTIR results three months after their fabrication, although they were not reported here). Each plot presents the EO (green), the emulsion (black), the Eumulgin surfactant (blue), and the distilled water (red) spectra for a direct comparison, in agreement with the upper legends. The lower horizontal axis corresponds to the wavenumber ($k = 2\pi/\lambda$), as reported by the FTIR instrument, while the upper horizontal axis shows the wavelength (λ), to facilitate the interpretation of the spectrum. On the vertical axes of the left and right, transmittance and absorbance percentages (%T and %A) are reported, respectively, to facilitate reading. Each plot depicts some of the relevant wavenumbers corresponding to certain chemical groups that are relevant to the analysis of the NE composition. In both plots, the spectrum of Eumulgin shows a band at 2922 cm^{-1} corresponding to the O-H stretching of the carboxylic acid. Around 1732 cm^{-1}, a stretching C=O vibration is also produced in the acid group. At 1097 cm^{-1}, a noticeable band corresponds to a C-O stretching of the carboxylic acid of Eumulgin. The water spectrum shows two typical bands at 1639 cm^{-1} and 3329 cm^{-1}.

Palmarosa EO presents a spectrum very similar to that published by [38,45], despite using different concentrations of EO and surfactant (Tween 80). Geraniol corresponds to the main component of the essential oil of palmarosa. A broadband can be observed at 3331 cm^{-1}, associated with the O-H stretching of the alcohol group. The C-H tension of the alkane and alkene groups is also observed in the range between 2800 and 3000 cm^{-1}. The narrow band at 997 cm^{-1} corresponds to the C-O stretching of the alcohol group. Furthermore, at 1639 cm^{-1}, a C=C stretching vibration is observed. The most similar result corresponds to the emulsion with 6% of EO, which is comparable to our 5% emulsion. Here, a broadband is formed at 3329 cm^{-1}, which can be attributed to the stretching of O-H corresponding to the continuous phase of distilled water of the emulsion (superposed with the band at 3331 cm^{-1} of the alcohol group in geraniol). The displacement of this band from 3275 cm^{-1}, as observed in distilled water, to 3129 cm^{-1} could have occurred due to the intermolecular interaction of the O-H group. The band at 1639 cm^{-1} corresponds to the stretching of C=O. Both the surfactant and palmarosa EO presented with bands in this region, which increased in the emulsion due to the presence of water, and with interactions between the surfactant and the continuous medium. Another relevant band is observed at 1097 cm^{-1}, which tends to absorb more at higher concentrations of surfactants [45].
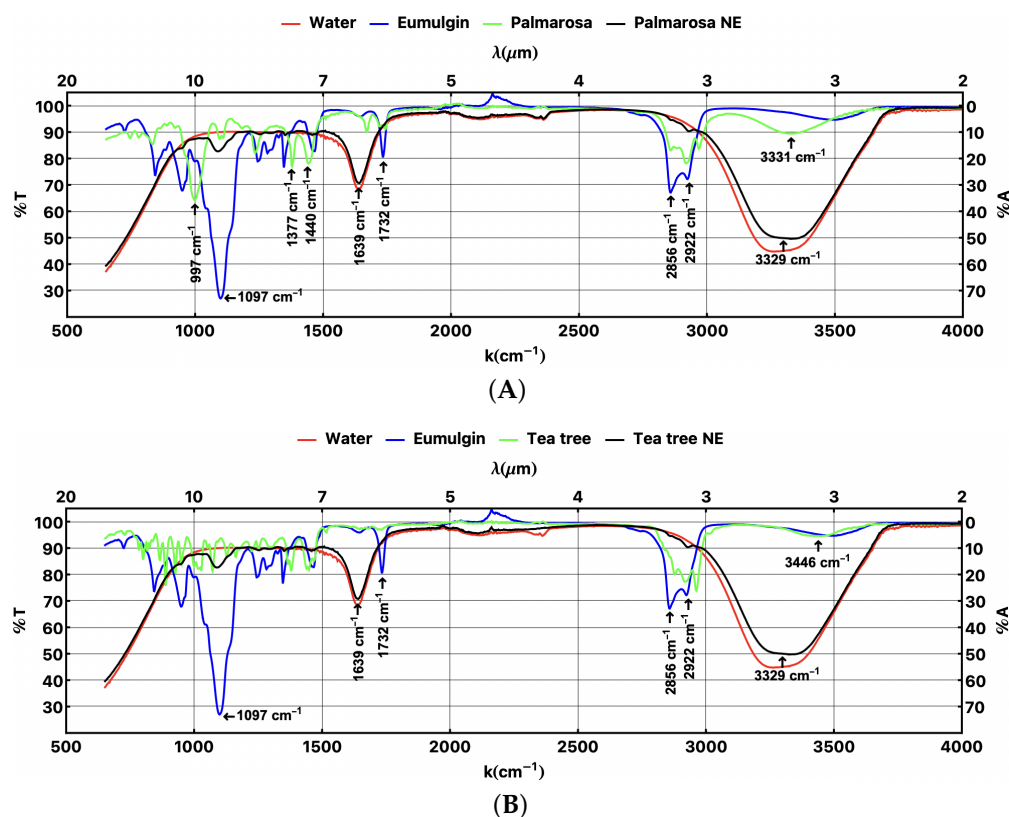
Figure 2. FTIR analysis of (**A**) palmarosa EO (green) and emulsion (black), and (**B**) tea tree EO (green) and emulsion (black). Both are also compared with the Eumulgin emulsifier (blue) and distilled water (red).

In contrast, the tea tree EO presented with a similar spectrum as that seen in some terpinen-4-ol databases [67]. Since this compound corresponds to approximately 70% of the EO, the FTIR results confirm its presence. The spectrum shows a broadband at 3446 cm^{-1} corresponding to the O-H stretching (inherited from NE but partially superposed with the band at 3329 cm^{-1} coming from water). Similarly to the palmarosa spectrum, C-H stretching is produced between 2800 and 3000 cm^{-1} due to the presence of alkane and alkene groups. Different flexions of O-H are observed in ~1430 cm^{-1} and ~1380 cm^{-1}. The tea tree oil emulsion shows almost the same spectrum as the palmarosa one. In both NEs, a band with low absorption is seen around 2100 cm $^{-1}$, which is not present in any of the EOs and surfactants, nor on water spectra. This specific band could be associated with interactions between the components of the emulsions. As can be observed, the main bands of the Eumulgin and EOs are present in some cases in the NEs but at a lower intensity, because the emulsion is mainly composed of water, which interferes with the measurement of the other components.

NEs show the main alcoholic compounds in relation to each EO studied, increasing their antimicrobial activity through the presence of the corresponding alcoholic groups (k = 3331 cm^{-1} for palmarosa and k = 3446 cm^{-1} for tea tree). They promote the lipophilicity of the compounds responsible for the antimicrobial properties of EOs, allowing the compound to bind to specific sites, thus disrupting cellular processes.

For palmarosa EO, its composition and characterisation, as reported in this work, corresponded with other studies in the literature [38,45]. Compared to [38], the main bands were observed as having slight shifts in the bands around 1442 and 2924 cm^{-1} for those in 1440 and 2916 cm^{-1}, respectively. For the tea tree oil, another study [68] is comparable to ours, especially in the range of 2900 cm^{-1}.

3.1.3. Initial Droplet Size Characterisation

The initial analysis of droplet size through DLS showed that the palmarosa emulsion, with 5% EO, had an average droplet size of 11.4 nm, with a PDI_a of 0.2256. In the case of the tea tree emulsion with 5% EO, its average droplet size was 10.9 nm and its PDI_a was 0.1554 [69]. The analysis of the droplet size, using DLS, of EO 10% emulsions showed that the size distribution was greater than that of the 5% emulsions. In the case of the 10% emulsion of palmarosa, the initial average droplet size was measured at 14.7 nm with a PDI_a of 0.5159. On the other hand, the tea tree emulsion with 10% EO presented a mean droplet size of 16.9 nm with a PDI_a of 1.507. This confirms droplet sizes on the nanoscale, as suggested by the turbidity tests. The initial characterisation parameters are reported in Table 1 for turbidity, the average size of the droplets, and for PDI_a, as obtained just after fabrication for each NE.

Table 1. Initial droplet size characterization and polydispersity obtained for palmarosa and tea tree emulsions at different concentrations.

EO	Conc.	Turbidity (NTU)	Av. Size (nm)	PDI_a
Palmarosa	5%	34.6	11.4	0.23
	10%	53.5	14.7	0.52
Tea tree	5%	33.8	10.9	0.16
	10%	50.6	16.9	1.51

3.2. Droplet Size Distribution Follow-Up and Its Stability

3.2.1. Long-Lived Droplet Size Stability over Time for the 5% Emulsions

The droplet size distribution and the polydispersity changes for the 5% emulsions were studied over different periods for palmarosa and tea tree EOs, at 1, 3, 6, and 12 months after their initial preparation. The DLS results are shown in Figure 3A (palmarosa) and B (tea tree), with solid lines in colours in agreement with the legend on the right side. Each curve is an adjusted spline from the data provided by the equipment using the size distribution by number mode. The gridlines on the horizontal axis each represent 5 nm and follow a logarithmic scale.

As seen in Figure 3A, the palmarosa emulsion remained stable with droplet sizes varying around their peaks, which were almost statically located between 9 nm and 11 nm. Although no phase separation processes occurred, the droplets of the emulsion slightly changed over time, with changes that were not statistically significant considering their dispersion. Between the 3-month and 6-month measurements, the peak droplet size distribution decreased from 9.6569 nm to 8.6398 nm (a reduction of 1.0171 nm), much less than one standard deviation. Furthermore, between 6 and 12 months, a non-meaningful increase in droplet size occurred. In contrast, Figure 3B corresponds to the tea tree emulsion, which remained stable between 8 and 10 nm for its peak diameter distribution. Similarly to palmarosa, the tea tree emulsion exhibited a droplet size reduction between 3- and 6-month follow-ups. The reduction was 2.04 nm for the peak droplet size diameter distribution, which was still not statistically significant. Both emulsions followed this stable trend during the one-year follow-up. The samples were kept at room temperature without any special storage care other than darkness. However, the laboratory where the nanoemulsions were commonly manipulated is a facility with partial control of temperature; this warrants fluctuations no higher than $\pm 5\,°C$ around $25\,°C$.
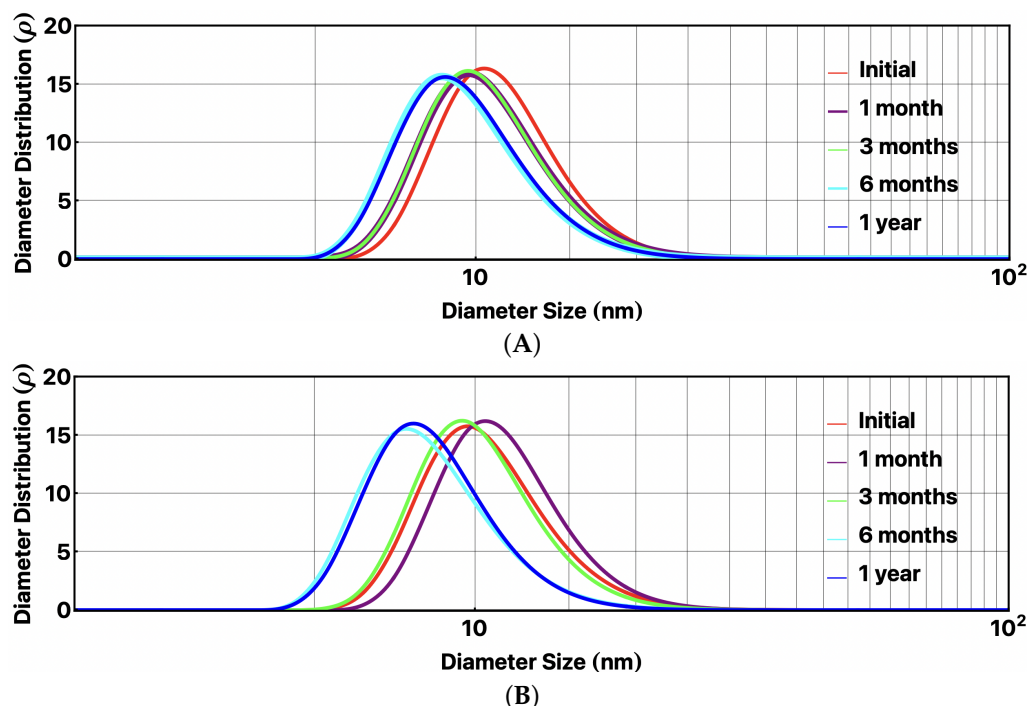
Figure 3. Diameter distributions of (**A**) palmarosa and (**B**) tea tree 5% emulsions studied over time. The gridlines corresponding to the horizontal axis each represent 5 nm and follow a logarithmic scale.

Table 2 reports the maximum number of particles (peak) from the statistical distribution with a specific diameter, considering the characteristic diameter (Max). In addition, the mean diameter (μ) and the standard deviation (σ) are also reported. The difference between the characteristic diameter and the mean diameter shows a positive distribution skewness that is maintained at all times for both samples. Considering the stability, the characteristic diameter becomes statistically stable over time in both cases, remarking the higher kinetic stability. The tiny non-meaningful variations observed are commonly attributed to additional factors such as evaporative ripening, Ostwald ripening, and the changes in the surfactant concentration that have been observed for NEs and MEs [70].

Table 2. Follow-up of characteristic droplet size and stability parameters (maximum distribution, mean, standard deviation, the two PDIs, and zeta potential (ζ) for both 5% NEs.

| EO	Time	Max. (nm)	μ (nm)	σ (nm)	PDI_a	PDI_b	ζ (mV)
Palmarosa	Initial	10.37	11.45	3.15	0.28	0.23	−1.08
	1 month	9.76	10.87	3.19	0.29	0.21	−1.09
	3 months	9.66	10.81	3.13	0.29	0.19	−1.09
	6 months	8.64	9.85	3.01	0.31	0.18	−1.12
	1 year	8.82	9.94	3.00	0.30	0.18	−1.11
Tea tree	Initial	9.76	10.88	3.26	0.30	0.16	−2.11
	1 month	10.47	11.58	3.24	0.28	0.18	−2.31
	3 months	9.46	10.49	3.00	0.29	0.18	−2.46
	6 months	7.42	8.49	2.60	0.31	0.24	−2.67
	1 year	7.65	8.57	2.48	0.29	0.22	−2.95

The droplet size distributions exhibit a consistent uniformity, with diameters approximately ranging from 5 nm to 30 nm (see Figure 3). Note in particular that, for the tea tree NE, a characteristic diameter reduction is reached one year later, while the droplet size range is broadened in terms of polydispersity (Figure 3B). This last phenomenon

is practically not present in the palmarosa NE. It is important to note that, when using different equipment, the determination of PDI varies.

The zeta potential (ζ) provides certain evidence of the stability of the droplets against sedimentation, aggregation, and coalescence. For ionic surfactants, higher absolute values of zeta potential (above 30 mV) indicate repulsion between droplets, increasing the stability [71]. In contrast, for non-ionic surfactants such as Eumulgin, absolute values close to zero (below 10 mV) are expected because of the double layer of steric repulsion [72–74]. The tracked values in Table 2 for the zeta potential were obtained as the average of a three-fold test. The tiny variations are commonly attributed to impurities [75,76].

3.2.2. Initial Droplet Size Stability Behaviour Compared at Two Different EO Concentrations

As a comparative analysis for the fabrication method, alternative NEs at a concentration of 10% (w/w) were also initially analysed during the first three months; they exhibited a similar stability behaviour, predictive of long-lived stability, but we still suggest a more detailed parametric analysis in future work, in terms of EO concentrations. Figure 4 shows the differences in droplet size distributions for both concentrations, from initial preparation to 3 months after, for palmarosa NEs (Figure 4A) and tea tree NEs (Figure 4B). The dotted lines correspond to the 5% concentrations of NEs, while the continuous lines correspond to the 10% concentrations of NEs. In the following section, we use the nomenclature $O_{C\%}$ to refer to the different NEs, with O=P, T for palmarosa and tea tree, respectively, and $C = 5, 10$ for the two concentrations of EO used (that is, $P_{5\%}$, $T_{5\%}$, $P_{10\%}$, and $T_{10\%}$).

(A)

(B)
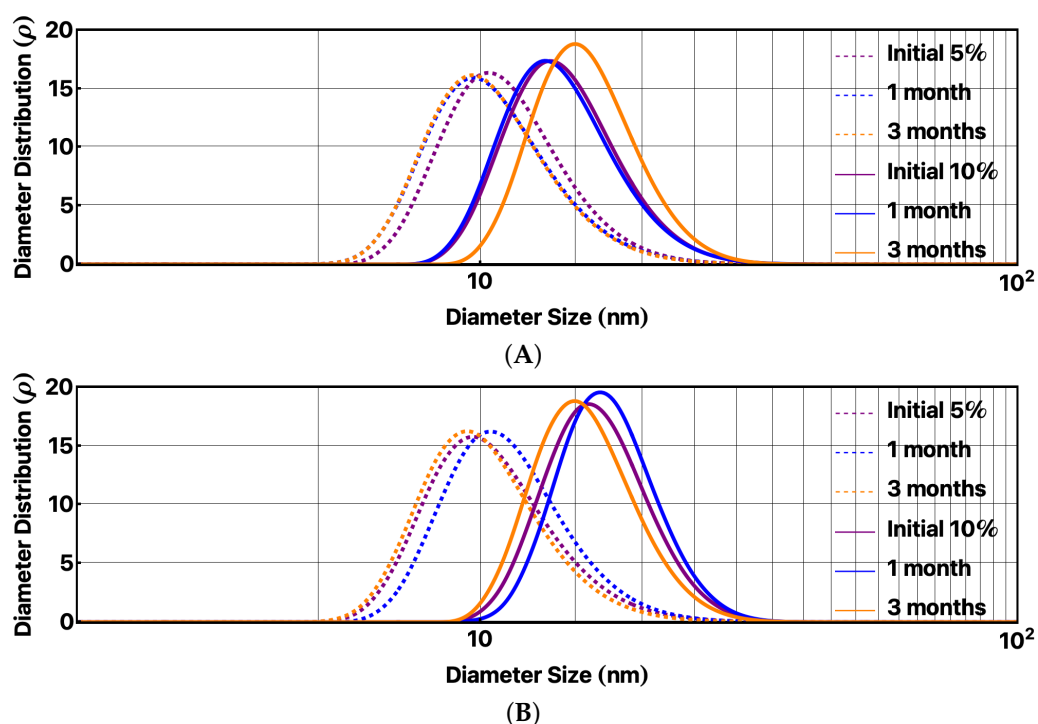
Figure 4. Diameter distributions of (**A**) palmarosa and (**B**) tea tree NEs studied at concentrations of 5% (dashed lines) and 10% (continuous lines) (w/w) over a period of 3 months. The gridlines corresponding to the horizontal axis each represent 5 nm and follow a logarithmic scale.

Comparative increases of 3 nm and 6 nm were respectively observed for the droplet size diameter of each EO as a function of a higher concentration. This is consistent with the behaviour for similar emulsions made using lemon oil [77]. In both Figure 4A,B, positive skewnesses are observed; however, these are reduced for the 5% NEs. The $P_{10\%}$ NE shows a slight change in the average initial droplet size in diameter, from 11.4 to 14.7 nm, between

the concentrations. For tea tree, there is a corresponding higher increase in the average initial diameter of the droplet, from 10.8 to 16.0 nm.

Palmarosa NEs present slightly different behaviour over time between $P_{5\%}$ and $P_{10\%}$. Although it is not significant, $P_{5\%}$ demonstrates some reduction over time in the characteristic droplet diameter. $P_{10\%}$ has a characteristic diameter increase; it increases from the initial droplet size of 14.7 nm, then decreases slightly after one month to 14.5 nm, and, after three months, increases to 16.0 nm. There is a slight reduction in the heterogeneity of the sample, while its skewness tends to reduce in general. For comparison, in [70], several lidocaine NEs with different concentrations were studied over time, observing a characteristic diameter reduction after 6 months in 44% of their samples.

The behaviour of the tea tree NE over time for both concentrations is similar. For both concentrations, the NE increases its droplet size after one month and then decreases three months later. Specifically, in the case of the $T_{10\%}$, the initial characteristic droplet size was 16.0 nm; then, after one month, it was 16.8 nm; finally, three months later, it reduced to 15.0 nm. However, as before for the $P_{5\%}$, those changes are non-meaningful for both EOs due to their dispersion, thus exhibiting high stability (see Table 2).

3.2.3. Polydispersity Stability Analysis for the 5% NEs

The 5% NEs were analysed over time to monitor changes in droplet size polydispersity as an additional parameter to track group stability. Figure 5A (palmarosa NE) and B (tea tree NE) illustrate the integrated behaviour of droplet size characterisation and polydispersity for $P_{5\%}$ and $T_{5\%}$, tracking the slight changes over time (see Table 2). The vertical axis represents the mean diameter obtained from the distribution (highlighting dispersion with vertical arrows to exhibit the statistical droplet size stability), while the horizontal one reports the characteristic diameter in nanometres. Each measure is reported using a disk whose size illustrates (at a different scale than the axes) the range of diameters (in nanometres) containing 99% droplets. Finally, PDI_a is observed in colour. The disk sizes, times, and PDI_a colours agree with the legend around.

Figure 5A shows different ranges on each axis for the reported values. Thus, the characteristic diameter (peak) decreases below the mean diameter value, revealing an asymmetric droplet size distribution with a higher proportion of particles larger than the mean (positive skewness). Both mean and characteristic diameters show non-meaningful oscillations over time. This reduction has been observed as a consequence of evaporation after stirring [78]. Thus, the polydispersity is lower for a more homogeneous distribution with larger but unstable droplets. In this process, some energy is exchanged, but it is exchanged around a stable equilibrium point. Several months afterwards, the range of droplet size distribution drops from 16 to 15 nm, resulting in a more uniform distribution. Despite this, the PDI_a (σ/μ) shows only tiny variations over time.

Figure 5B, for the tea tree NE, exhibits a similar general behaviour between the characteristic (peak) and the mean diameters, revealing a positive skewness and presenting more large-sized particles than smaller ones. An increase in the diameter distribution is observed during the first month, then decreases, as in the palmarosa case. The reduction in diameters is more noticeable than for palmarosa; it is due to the fracturing of unstable droplets into smaller but more stable droplets. The characteristic diameter after six months reduces to below 8 nm. It has an impact in the 99% size range for the diameter droplets, showing a more homogeneous size distribution around the mean. Note again the final increase of PDI_a as a result of a faster decrease in μ than σ. In any case, those tiny variations become non-meaningful in spite of the larger dispersion.
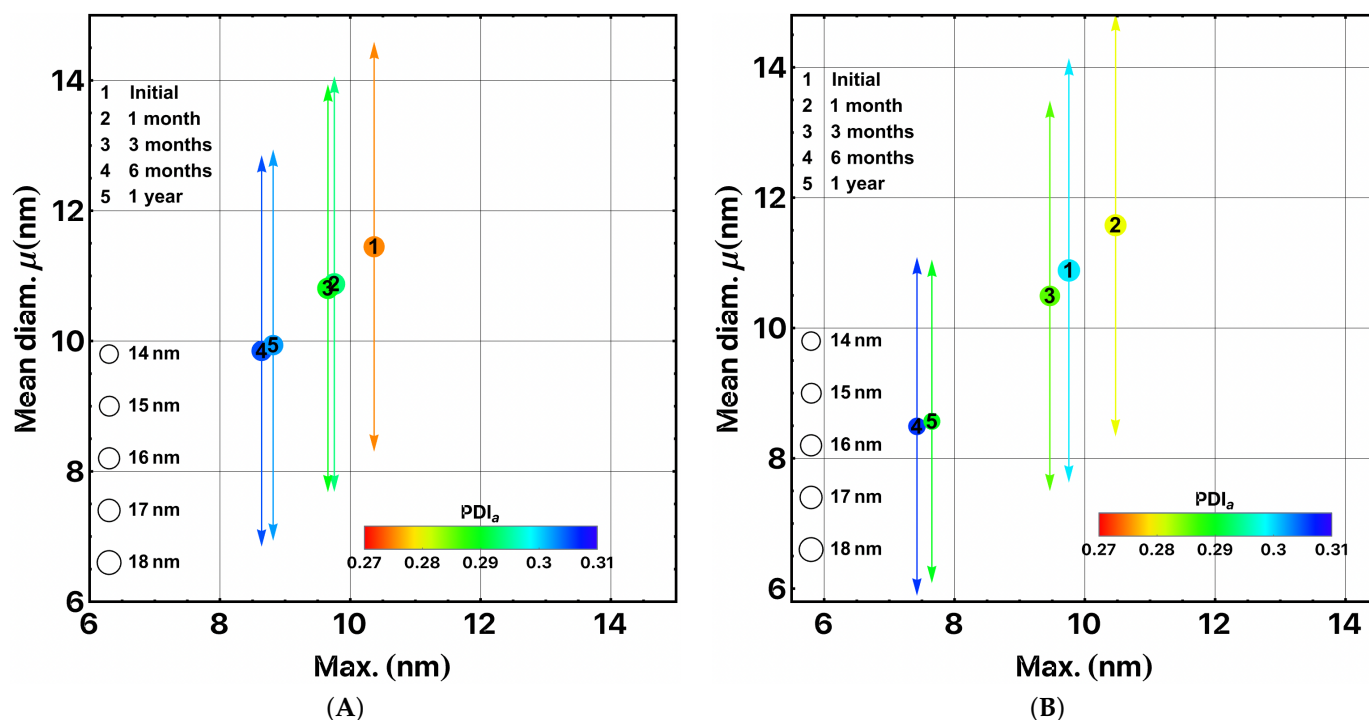
Figure 5. Comparison between the characteristic (horizontal) versus the mean diameter (vertical) in the NE, including its dispersion, shown with arrows ($\pm\sigma$) for (**A**) palmarosa and (**B**) tea tree (see Table 2). NEs are studied over time in agreement with the numbering; the disk radius reports a 99%−range of distribution, while the colour reports the PDI_a value (see the attached legends).

3.2.4. Thermoresponsivity Insight Analysis for the 5% Emulsions

A complementary study of droplet size thermoresponsivity was developed for NEs with concentrations of 5%. It was carried out on samples following one year of tracking. Following an initial DLS analysis at room temperature, the samples were then stabilised by the equipment at 50 °C. Then, a DLS spectrum was recorded every 10 min, keeping that temperature until the plot stabilised. Finally, the samples were allowed to cool to room temperature, while the spectrum was again recorded every 10 min during the cooling until the plot stabilised.

Figure 6 shows the distributions for each stage, with the measurement time differentiated by colour, according to the legend. Figure 6A,B correspond to the palmarosa NE (sustained heating and cooling, respectively), while Figure 6C,D correspond to the tea tree NE. A logarithmic scale is used for the diameter on the horizontal axis, while the vertical axis reports the value of the distribution. The vertical lines report diameters in intervals of 10 nm.

The palmarosa NE is shown in Figure 6A; its initial characteristic distribution is shown by the black dotted line, followed by colour distributions for the NE at 50 °C (10, 20, . . . , 60 min) from blue to red, as the time advances up to 60 min. Notice a general non-monotonous droplet size increase for the characteristic diameter. The inset on the right shows an incipient group of much larger-diameter particles (between 100 and 1000 nm). The 20 min distribution should be highlighted, which, although it shows a reduction in the trend of increasing characteristic droplet size, also exhibits a shift in the distribution to the right. This can be explained as due to the particles more able to coalesce being the larger ones, thus resulting in the peak distribution shifting to the left for the more stable droplets. This phenomenon is repeated for the final distribution, at the expense of a notable secondary distribution towards 1000 nm. The cooling (Figure 6B) results in a rapid recovery of the original distribution (10, 20, . . . , 70 min), but only until a slow

final stabilisation (black dotted line) is obtained one day later. This analysis exhibits an interesting transport phenomenon; in particular, it reveals the dynamic process at the constant temperature of 50 °C, which surely is not reached uniformly as assumed by the temperature equipment sensor, due to the inhomogeneity of the mixture being analysed. This distribution is remarkably consistent with the initial distribution obtained during the analysis in Figure 6A.

Figure 6C,D for the tea tree NE show a similar phenomenon, with a faster but more modest thermoresponsivity, which rapidly becomes static at 50 °C. During cooling, recovery is slower; even at the end of stabilisation, the characteristic droplet size is a little above the initial value of the test (black dotted line in Figure 6C), at the expense of a much larger group in the inset. This is also true for the final stabilised distribution (black dotted line in Figure 6D, obtained two days after the main test), with a slightly higher value than the initial.

In summary, Figure 7A,B show the thermoresponsive dynamics for palmarosa and tea tree NEs. Each synthesises the behaviour of the mean diameter (Mean diam, shown in blue), the characteristic diameter (Max diam, shown in yellow), and the mean volume of the droplets (Mean vol, shown in green). They provide a better illustration of the transport phenomenon between droplets when the NE is kept at 50 °C outside of thermodynamic equilibrium. Figure 7A, of the palmarosa NE, shows the small increase in distributions gradually achieved in the first 60 min. The noticeable increase in volume shows an effective flow of droplets in coalescence. However, the recovery of the NE is observed when it is returned to room temperature. Figure 7B, of the tea tree NE, shows a more modest dynamic. It is remarkable that the small group of droplets over 1 μm remaining after the test only suggests kinematical stability rather than thermodynamic stability. Thus, both tests highlight a broad kinetic balance despite the moderate heating of the NEs. In the overall test, the selected temperature of 50 °C corresponds to an extreme temperature to which a commercial NE could be exposed.
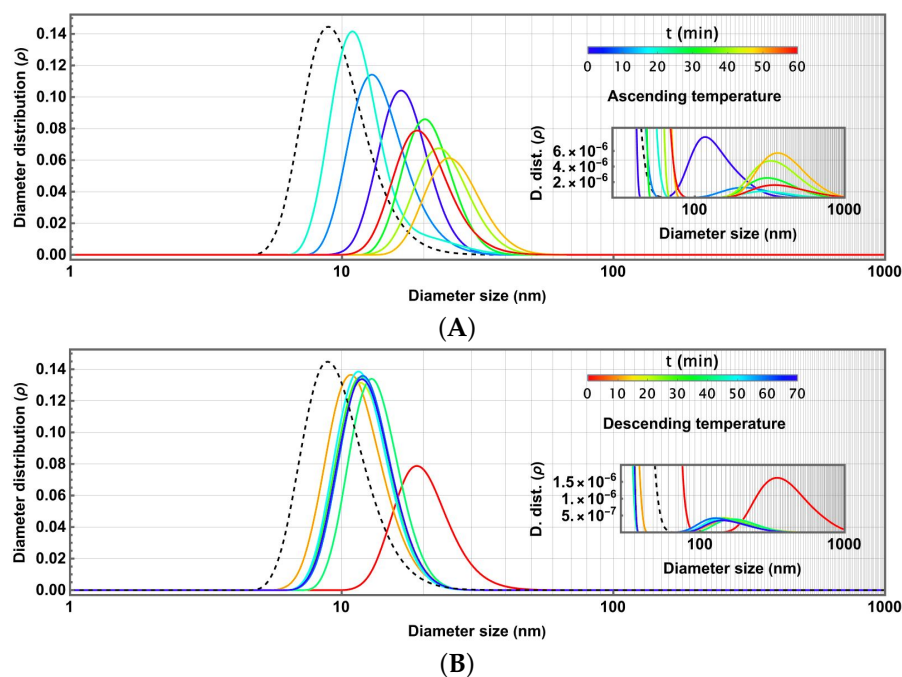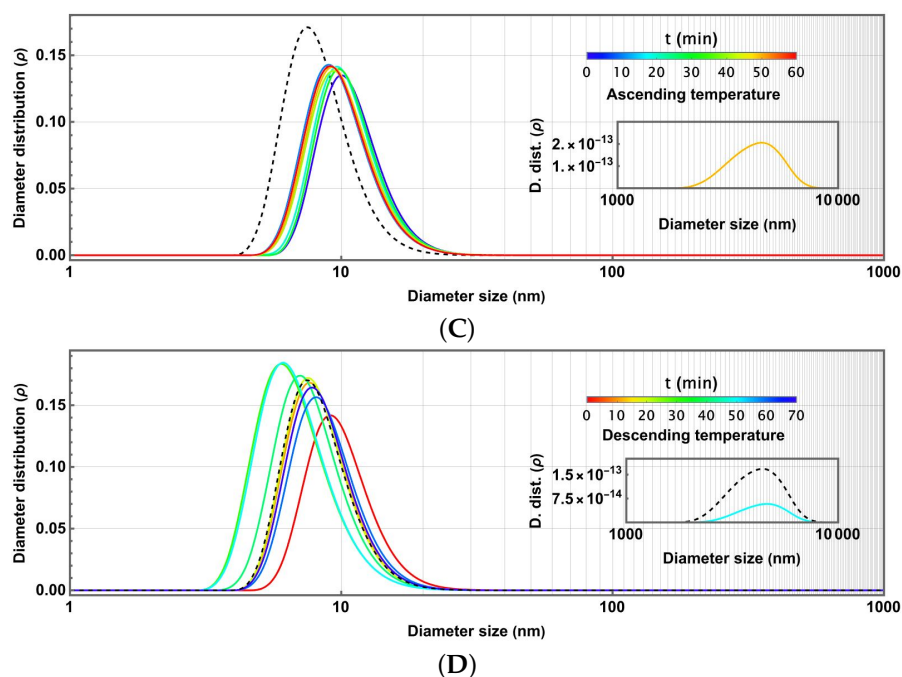

(A)

(B)

Figure 6. *Cont.*

Figure 6. Diameter distributions under a cycle of 18–50–18 °C heating–cooling phases for 5% emulsions. (**A**) Palmarosa at 50 °C, (**B**) palmarosa cooling from 50 °C to 18 °C, (**C**) tea tree at 50 °C, and (**D**) tea tree cooling from 50 °C to 18 °C. Each line colour is in agreement with the colour-bar above indicating the elapsed time. Black dotted lines correspond to the droplet size distribution at the initial temperature of the test, $T = 18°C$.
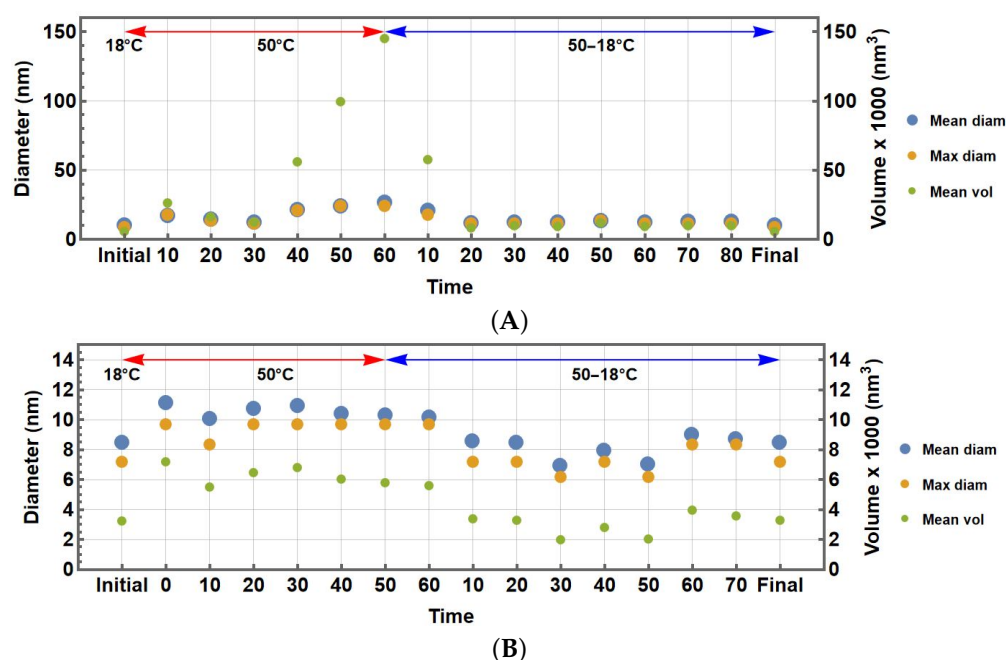
Figure 7. Mean and characteristic diameters, together with mean volume, for droplets under a cycle of 18–50–18 °C heating–cooling phases for 5% emulsions. (**A**) Palmarosa and (**B**) tea tree.

3.2.5. Final Remarks on the Droplet Size Stability Outcomes

A previous study [45] developed palmarosa NEs at different concentrations of surfactant (Tween 80) and EO. The smallest droplet size was obtained for a concentration of 2.5% of EO and 10% of surfactant. Using a different surfactant, the emulsifying capacity and stability were modified. In the current study, we achieved a similar droplet size using a higher concentration of surfactant and EO, reaching a high kinetic stability. Even for the

case therein, with a higher concentration, ours was four times the one previously reported there, obtaining a similar and stable droplet size [45].

An alternative study [79] obtained a palmarosa NE using citric acid and Tween 80. Their formulation did not have stability without citric acid, representing a key factor for obtaining an effective NE. The citric acid-containing emulsions contained 0.5% of EO and 1% of Tween 80, presenting a stabilisation process similar to our NEs over time. Initially, they obtained a droplet size of 36.2 nm, which reduced over time, 4 weeks later, to 15.3 nm. They also analysed the turbidity of their NEs over time, obtaining an initial value of 18.4 NTU and, 4 weeks later, a value of 2.7 NTU. However, turbidity considers not only the droplet size of the NE but also its concentration. In the case of that previous study, the composition of surfactant and EO corresponded only to 1.5% of the NE. In our case, the components corresponded to 18% and 31% of the NE, at 34.6 and 53.5 NTU, respectively, for the palmarosa emulsions.

3.3. Antibacterial Effectiveness at Several Concentrations Including Further Dilutions

The disk diffusion method was used to establish the efficacy of NEs against bacterial strains of *Salmonella* spp. and *B. subtilis*. The preparations are illustrated in Figure 8A for *Salmonella* spp. and B for *B. subtilis*. In each panel, the upper left corresponds to $P_{5\%}$, the upper right corresponds to $P_{10\%}$, the lower left corresponds to $T_{5\%}$, and the lower right corresponds to $T_{10\%}$. Each agar plate has five disks: the upper left is the control disk, the upper right is ampicillin as an antibiotic, the central disk is the NE studied, the bottom left is a post-prepared 50% (*v*/*v*) dilution and the bottom right is the 25% (*v*/*v*) dilution.

(**A**)　　　　　　　　　　　　　　(**B**)
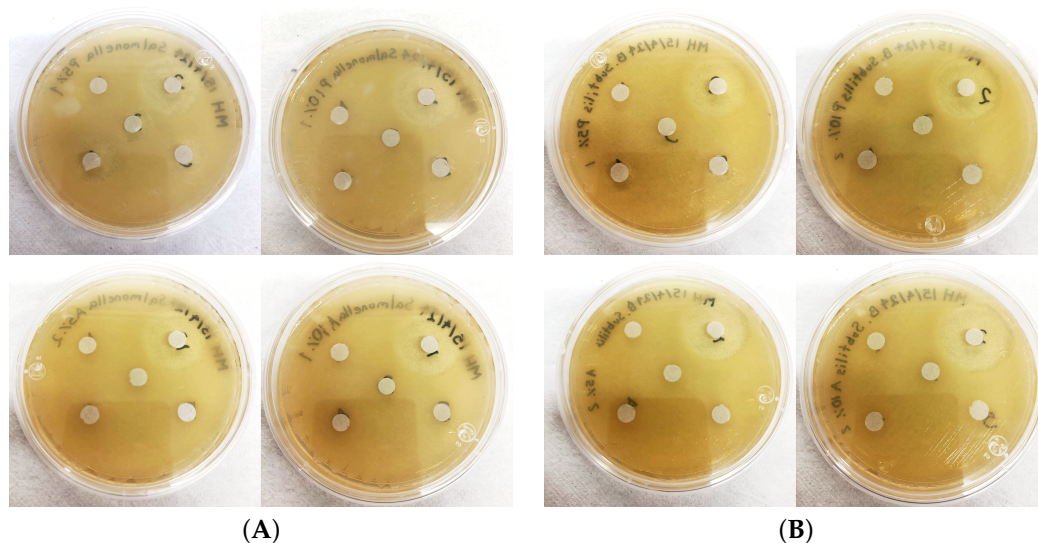
Figure 8. Disk diffusion preparations for (**A**) *Salmonella* spp. and (**B**) *B. subtilis*. The upper left denotes $P_{5\%}$, the upper right denotes $P_{10\%}$, the bottom left denotes $T_{5\%}$, and the bottom right denotes $T_{10\%}$. Each one has five disks for the control (upper left), the antibiotic (upper right), the NE studied (centre), the 50% (*v*/*v*) dilution (bottom left), and the 25% (*v*/*v*) dilution (bottom right).

Table 3 summarises the results for the diameter of the bacterial inhibition in cm for each preparation within the agar plate. The bacteria analysed are on the left side of the table. Each agar plate is shown in each column, corresponding to the palmarosa (P) and tea tree (T) NEs. The essential oil concentration is shown as a subscript. Although two experimental repetitions were performed as a control, only their average is included in the table. Each row corresponds to the treatments (S): the blank (or control not loaded), the antibiotic, and the NE, together with two post-prepared dilutions. As expected, the antibiotic had a much bigger inhibition zone than the NEs.

Table 3. Average inhibition diameters obtained from a pair of experimental repetitions for *Salmonella spp.* and *B. Subtilis* in cm for P$_{5\%}$, P$_{10\%}$, T$_{5\%}$, and T$_{10\%}$ for the following: blank sample, ampicillin (AB), NE, and its dilutions to 50% and 25%.

Bacteria	S	P$_{5\%}$	P$_{10\%}$	T$_{5\%}$	T$_{10\%}$
Salmonella spp.	Blank	0.67	0.68	0.66	0.66
	AB	2.56	2.55	2.50	2.54
	NE	1.39	0.92	0.78	0.77
	50%	1.57	0.73	0.81	0.81
	25%	1.06	1.05	0.72	0.68
B. subtilis	Blank	0.66	0.68	0.66	0.66
	AB	2.62	2.56	2.56	2.68
	NE	1.06	0.78	0.80	0.81
	50%	0.89	0.73	0.76	0.71
	25%	0.88	0.71	0.73	0.71

The information in Table 3 shows that palmarosa NEs had, in general, a bigger inhibition zone than the tea tree NEs, particularly for *Salmonella* spp. Although some tea tree NEs did not show notable inhibition zones, it was useful to show that their main components practically did not notably affect the bacteria, nor the Eumulgin compounds. Thus, the difference in the main components of both essential oils produces a different effect on bacteria. In particular, P$_{5\%}$ presented a deeper antibacterial effect than its P$_{10\%}$ counterpart, attributed to the difference in the size of the NE droplet.

A synthetic representation of the data in Table 3 is included for the analysis in Figure 9. These circular plots are shown in quadrants (the same as those in Figure 8) and each one of the columns is represented (by pairs comprising the repetitions in the same analysis group) as follows: palmarosa (C.M., upper quadrants) and tea tree (M.A., lower quadrants), 5% (left) and 10% (right) in both cases. Thereafter, the average inhibition diameter $d_g = \frac{1}{2}(d_g^1 + d_g^2)$ for the repetitions was obtained and plotted for each group or treatment g considered (blank, antibiotic, NE, NE 50%, and NE 25%). The following dispersion measure for each case was also obtained:

$$\Delta_g = \frac{|d_g^2 - d_g^1|}{d_g} \tag{1}$$

In each quadrant, d_g is reported as a circular arc for the group mentioned in the upper right colour legend. In each case, if $\Delta_g > 0.15$ (a midpoint in the variability commonly reported for the manually prepared disk diffusion tests [80]), the arc was plotted as a dashed line representing the most variable results between the cultures. Clearly, ampicillin had the highest effect against both bacteria in all agar plates compared to the NEs. However, the external black circle reports the extreme diameter provided by the antibiotic, but is jointly scaled for the four quadrants. In addition, the black central disk represents the blank diameter d_b (which is the same for all cases). Thus, diameters are reported in units of d_a (for this reason, the plots do not include absolute measures) using a logarithmic scale. Thus, the grey arcs in each quadrant correspond to $3/10, 4/10, \ldots, 9/10$ of d_a. Figure 9A,B correspond to *Salmonella* spp. and *B. subtilis*, respectively. Thus, all NEs and their dilutions exhibited an antibacterial effect on both bacteria at the same scale as the antibiotic.
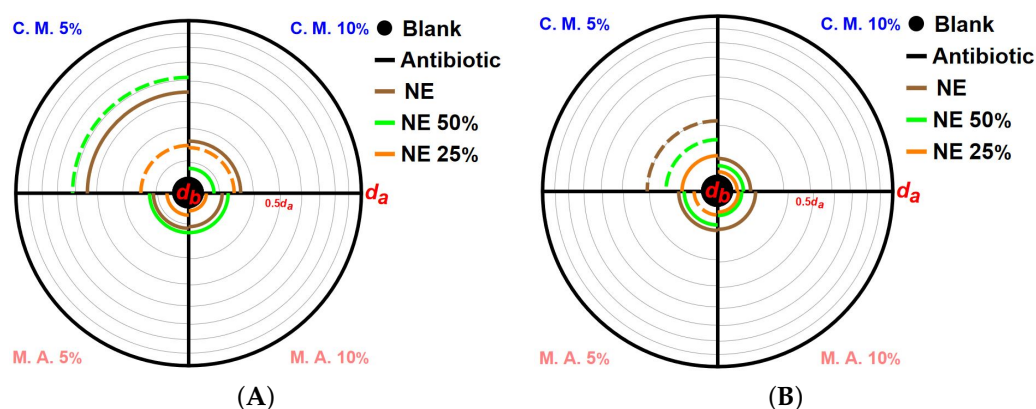
Figure 9. Comparison between inhibition diameters using (**A**) *Salmonella* spp., and (**B**) *B. subtilis*. Diameters for the antibiotic and blank cases, d_a in d_b, are jointly scaled. The colour legend describes the different treatments. A dashed arc reports a larger variation $\Delta_g > 0.15$ within the repetitions.

The inhibition zone reported in the second quadrant (upper right) for $P_{10\%}$ and *Salmonella* spp. is significant, despite depicting a mild variation (see Table 3). In general, the inhibition diameter was related to the dilution of the sample. In that significant quadrant for *Salmonella* spp., the diameter was larger for NE 50% than for the direct NE. The behaviour was more limited for $P_{10\%}$ and higher for the direct NE. In contrast, for *B. subtilis*, although lower than in the previous case, the antibacterial effect was greater for the direct NE than for the 50% dilution, but it remained significant for $T_{5\%}$. In general, more modest results were observed for the tea tree NE. The different effects of NEs on both types of bacteria are attributed to the amphiphilic properties of the droplets. In addition to the larger surface area generated by the reduction in droplet size between 5% and 10% NEs, the reduction in cell surface area leads to greater cell rupture, caused by a decrease in the equilibrium of the cell membrane, which leads to material loss [1,81,82]. The antimicrobial effect of the NE reported in other quadrants is similar, almost independent from the EO and their dilution.

As seen in Figure 9A, in the significant second quadrant, the efficacy of the palmarosa 50% NE had a similar effect to the original NE, but a greater effect than the 25% dilution. In fact, *Salmonella* spp. has a hydrophobic outer membrane that allows EO to enter the cell, although such an effect is partially reduced as a function of the amount of water due to the availability of the EO. Thus, the greater inhibition of Gram-negative bacteria in *Salmonella* spp. is believed to be due to the nanoemulsified EO [82–84] and is also attributed to the composition of the cell membrane and its affinity for the constituents of the EO [1,82]. A different effect is seen for *B. subtilis*, which has a hydrophilic outer membrane, limiting the antibacterial effect of EOs, more notably in dilutions where the amount of EO is lower. Because the dilutions alter the proportion of oil to water, a superposed effect is acts together with the droplet size to enter the cell membrane. However, the result for $P_{5\%}$ still suggests an important effect of the nanoscale droplet size on that bacteria.

The antimicrobial activity of the NEs observed in this study showed interesting outcomes for the palmarosa NE at a concentration of 5% (*w/w*). It is relevant to note that the composition of the palmarosa EO showed a higher inhibition than the tea tree EO in its nanoformulated form. Several factors impact the efficacy of an NE and its antimicrobial activity, such as the droplet size, the chemical composition of the surfactant and the EO, and also the conditions of the experiment. In similar research on palmarosa NEs, the antibacterial susceptibility of their formulations was analysed, considering variations in the concentration of EO and surfactant, finding better results at higher concentrations of EO and with larger droplets (87 nm) [45]. In contrast to those results presented in that study, we showed that a higher concentration and a higher droplet size are not always the most

effective. Our results showed that a smaller droplet size (related to a smaller concentration) can have a higher bacterial susceptibility, which is more notable for palmarosa NEs. The components of the EO in the NE, the droplet size, and the surfactant properties improve the NE's penetration ability, as they comprise asynergistic effects enabling different inhibition mechanisms.

As a comparison, another study [1], using 50 μL/well of NE, obtained inhibition zones between 8.2 and 12 mm. These NE inhibition zones, compared to those for antibiotics, had inhibition ratios between the NE and the antibiotic control, totalling approximately 0.34 and 0.52 times, corresponding to the results obtained in our current investigation. In another study, the antibacterial effect of peppermint and myrtle NE was evaluated in *B. subtilis* and *E. coli* (Gram-positive and Gram-negative bacteria, respectively) [46]. Peppermint NE had a higher effect at a higher concentration on *B. subtilis*, while a lower concentration had a higher antibacterial activity on *E. coli*, similar to our analysis. The NEs had almost the same droplet sizes, but different concentrations within the NE respecting the continuous phase. This was a similarly notable result to that observed in the current study for palmarosa NEs.

4. Discussion

4.1. Composition Study

The slight differences found in the literature in both EO spectra could be produced by factors that affect the EOs' composition. These can vary according to the region, environmental conditions, or the harvest season. In [85], it was shown that the geraniol concentration present in palmarosa EO varied up to 10% depending on the harvest season. Thus, through the comparison and confirmation of the main bands of the EOs, we ensured that the active components responsible for the antibacterial activity were present after the ultrasonication process.

4.2. Droplet Size and Stability Study

4.2.1. Droplet Size Follow-Up and Long-Lived Stability

It should be noted that our study considered monitoring the stability of the NEs for one year, achieving high stability throughout this period. This behaviour contrasts with that commonly reported for the NEs regarding droplet sizes (for example, in [16]). One of the most relevant observations of the stability study is that polydispersity showed a certain dynamic through time, with small oscillations of about 2 nm. This provides important details about stability properties for interface nanofabrication for potential commercial usage. In particular, our insight thermoresponsive analysis demonstrated additional outstanding stability but also exhibited notable dynamics around the droplet size equilibrium, which should be further explored in future research.

4.2.2. Statistical and Physical Interpretation

The statistical interpretation of droplet size in NEs deserves a more detailed discussion of the findings from the temporal follow-up. The emulsion does not have a defined size in the diameters of the droplets; instead, it is a complex system in which many droplets of different sizes coexist, with an average size from its distribution (mean size) and a characteristic size (modal size). Because of its interfacial interactions, this system is subject to dynamic coalescence and flocculation processes, which are thermodynamically different for each droplet size. In this group of droplets, the largest are more susceptible to those processes. This dynamic is not uniform, especially over time in the face of the temperature changes driving it, even though the surfactant supports a metastable equilibrium process [55]. The dynamics of the statistical distribution usually showed variations over

time, with minimal oscillations or even a decrease in the value of the characteristic size at the expense of the coalescence of the larger droplets, except when the process was driven by temperature in a sustained way, as observed in the thermoresponsive study. Both behaviours are observed in the temporal follow-up of the NEs and their response to heating and cooling. In the cases of the NEs studied, the changes generated in the free energy, as discussed in Section 2.2.4, are not extreme enough to exit the metastable equilibrium, showing a good performance in the face of typically controlled changes, such as those to which a NE for commercial use could be subject.

4.3. Antimicrobial Properties

In the current study, Gram-positive bacteria such as *B. subtilis* underwent a greater inhibitory effect from direct NE due to their hydrophilic outer cell membrane affinity, where the dispersed phase blocks EOs. Several studies have reported that the antibacterial effect of EOs in coarse emulsions is higher in Gram-positive than in Gram-negative bacteria due to their hydrophilic membrane reducing penetration into the cells of the diluted oil [1,82]. As seen in Figure 9B, the largest inhibitory zone was observed for the original NEs without dilution. In contrast, Gram-negative bacteria have an hydrophobic outer membrane, making it easier for EOs to enter the cell, and this effect is improved at a nanoscale. Similar future tests are in order on other Gram-positive and Gram-negative bacteria.

5. Conclusions and Future Work

In the present study, several NEs with long-lived droplet size distributions were fabricated using palmarosa and tea tree EOs. The characteristic droplet sizes obtained for these NEs were between 8 and 15 nm, depending on the concentration of the NE and the EO. These NEs were elaborated using an ultrasonification-induced process to reach nanoscale droplet sizes without delayed stabilisation, as seen in other studies where the droplet size still tends to change over time. Those droplets became stable for large periods (month-long periods, up to one year) without special storage but with darkness at room temperature.

During the droplet size follow-up, an almost unperceived dynamic process was observed. Without meaningful modification of the droplet size distribution and polydispersity features, NEs showed a long-lived droplet size characterisation. Still, for the insight thermoresponsive test, which raised their temperature to 50 °C, they did become reversibly changed, despite dynamic changes being observed around a stable equilibrium. In future work, our samples should be tested using more extensive thermoresponsive analysis to obtain information, not only about the nature of the stability's strength and the dynamic behaviour of polydispersity, but also about transport comparisons between droplet sizes.

The limitations of our study should be given. Because the DLS method is based on spherical droplets, the aggregation processes may alter certain outcomes [86], broadening the droplet size distribution and, although less sensitive, causing a shift in the characteristic droplet size (peak). As an initial characterisation (not reported as central in this study), the morphology of the droplets was qualitatively reviewed using atomic force microscopy [87], which exhibited spherical droplets. Although tiny variations in the DLS spectra over time suggest a lower aggregation or flocculation phenomena assuming the initial morphology, the thermoresponsive test could generate aggregation because the morphology was not checked during the test, so this insight test could exhibit a lack of precision.

Despite the notable droplet size stability, the nanoscale droplets and composition allowed NEs to demonstrate antimicrobial activity against Gram-positive and Gram-negative bacteria, particularly highlighting the effect of the palmarosa NE. It would be important to extend these studies on the parametric dilution effect of NEs on different microorganisms.

In a future study, we will focus on the effects of NEs on a larger group of microorganisms, as well as their human biocompatibility.

Abbreviations

The following abbreviations are used in this manuscript:

ATR	Attenuated total reflectance
CAS	Chemical Abstracts Service
FDA	U.S. Food and Drugs Administration
FTIR	Fourier transform infrared spectroscopy
DLS	Dynamic light scattering
EOs	Essential oils
MEs	Microemulsions
NEs	Nanoemulsions
NTU	Nephelometric Turbidity Units
O/W	Oil in water
PDI	Polydispersity index

References

1. Krishnamoorthy, R.; Athinarayanan, J.; Periasamy, V.S.; Adisa, A.R.; Al-Shuniaber, M.A.; Gassem, M.A.; Alshatwi, A.A. Antimicrobial activity of nanoemulsion on drug-resistant bacterial pathogens. *Microb. Pathog.* **2018**, *120*, 85–96. [CrossRef] [PubMed]
2. Dey, D.; Chowdhury, S.; Sen, R. Insight into recent advances on nanotechnology-mediated removal of antibiotic resistant bacteria and genes. *J. Water Process. Eng.* **2023**, *52*, 103535. [CrossRef]
3. Mba, I.E.; Nweze, E.I. Nanoparticles as therapeutic options for treating multidrug-resistant bacteria: research progress, challenges, and prospects. *World J. Microbiol. Biotechnol.* **2021**, *37*, 108. [CrossRef] [PubMed]
4. Weisany, W.; Yousefi, S.; Razzak Tahir, N.A.; Golestanehzadeh, N.; McClements, D.J.; Adhikari, B.; Ghasemlou, M. Targeted delivery and controlled released of essential oils using nanoencapsulation: A review. *Adv. Colloid Interface Sci.* **2022**, *303*, 102655. [CrossRef]
5. Wang, Y.; Ai, C.; Wang, H.; Chen, C.; Teng, H.; Xiao, J.; Chen, L. Emulsion and its application in the food field: An update review. *eFood* **2023**, *4*, e102. [CrossRef]
6. Ozogul, Y.; Karsli, G.T.; Durmuş, M.; Yazgan, H.; Oztop, H.M.; McClements, D.J.; Ozogul, F. Recent developments in industrial applications of nanoemulsions. *Adv. Colloid Interface Sci.* **2022**, *304*, 102685. [CrossRef]
7. Mushtaq, A.; Wani, S.M.; Malik, A.R.; Gull, A.; Ramniwas, S.; Nayik, G.A.; Ercisli, S.; Marc, R.A.; Ullah, R.; Bari, A. Recent insights into Nanoemulsions: Their preparation, properties and applications. *Food Chem. X* **2023**, *18*, 100684. [CrossRef]
8. Ashaolu, T.J. Nanoemulsions for health, food, and cosmetics: a review. *Environ. Chem. Lett.* **2021**, *19*, 3381–3395. [CrossRef]
9. Gupta, A.; Eral, H.B.; Hatton, T.A.; Doyle, P.S. Nanoemulsions: formation, properties and applications. *Soft Matter* **2016**, *12*, 2826–2841. [CrossRef]

10. Jafari, S.; McClements, D. *Nanoemulsions: Formulation, Applications, and Characterization*; Elsevier Science: Amsterdam, The Netherlands, 2018.

11. Naseema, A.; Kovooru, L.; Behera, A.K.; Kumar, K.P.; Srivastava, P. A critical review of synthesis procedures, applications and future potential of nanoemulsions. *Adv. Colloid Interface Sci.* **2021**, *287*, 102318. [CrossRef]

12. Czerniel, J.; Gostyńska, A.; Jańczak, J.; Stawny, M. A critical review of the novelties in the development of intravenous nanoemulsions. *Eur. J. Pharm. Biopharm.* **2023**, *191*, 36–56. [CrossRef] [PubMed]

13. Touayar, M.; Zayani, R.; Messaoud, C.; Salman, H. Infuence of droplet size on the antibacterial efcacy of citral and citronella oil nanoemulsions in polysaccharide coated fresh-cut apples. *Sci. Rep.* **2023**, *13*, 10460. [CrossRef] [PubMed]

14. Wilson, R.J.; Li, Y.; Yang, G.; Zhao, C.X. Nanoemulsions for drug delivery. *Particuology* **2022**, *64*, 85–97. [CrossRef]

15. Aljabri, N.M.; Shi, N.; Cavazos, A. Nanoemulsion: An emerging technology for oilfield applications between limitations and potentials. *J. Pet. Sci. Eng.* **2022**, *208*, 109306. [CrossRef]

16. McClements, D.J. Advances in edible nanoemulsions: Digestion, bioavailability, and potential toxicity. *Prog. Lipid Res.* **2021**, *81*, 101081. [CrossRef]

17. Shiyu, H.; Jiaxuan, C.; Yeting, Z.; Yelu, W.; Tongtong, D.; Hangyan, S. Preparation of Stable Microemulsions with Different Droplet Size. *Am. J. Nanosci.* **2019**, *5*, 76–82. [CrossRef]

18. Kumar, N.; Verma, A.; Mandal, A. Formation, characteristics and oil industry applications of nanoemulsions: A review. *J. Pet. Sci. Eng.* **2021**, *206*, 109042. [CrossRef]

19. Sneha, K.; Kumar, A. Nanoemulsions: Techniques for the preparation and the recent advances in their food applications. *Innov. Food Sci. Emerg. Technol.* **2022**, *76*, 102914. [CrossRef]

20. Choi, S.J.; McClements, D.J. Nanoemulsions as delivery systems for lipophilic nutraceuticals: strategies for improving their formulation, stability, functionality and bioavailability. *Food Sci. Biotechnol.* **2020**, *29*, 149–168. [CrossRef]

21. Gauthier, G.; Capron, I. Pickering nanoemulsions: An overview of manufacturing processes, formulations, and applications. *JCIS Open* **2021**, *4*, 100036. [CrossRef]

22. Kumar, M.; Bishnoi, R.S.; Shukla, A.K.; Jain, C.P. Techniques for Formulation of Nanoemulsion Drug Delivery System: A Review. *Prev. Nutr. Food Sci.* **2019**, *24*, 225–234. [CrossRef] [PubMed]

23. Nazzaro, F.; Fratianni, F.; Martino, L.D.; Coppola, R.; Feo, V.D. Effect of Essential Oils on Pathogenic Bacteria. *Pharmaceuticals* **2013**, *6*, 1451. [CrossRef]

24. Rodrigue, K.C.T.; Djouhou, M.C.; Koudoro, Y.A.; Dahouenon-Ahoussi, E.; Avlessi, F.; Koko, C.; Sohounhloue, D.; Simal-Gandara, J. Essential oils as natural antioxidants for the control of food preservation. *Food Chem. Adv.* **2023**, *2*, 100312. [CrossRef]

25. Santamarta, S.; Aldavero, A.C.; Rojo, M.A. Essential oil of Cymbopogon martini, source of geraniol, as a potential antibacterial agent against Bacillus subtilis, a pathogen of the bakery industry. *F1000Research* **2023**, *10*, 1027. [CrossRef] [PubMed]

26. Abdi-Moghadam, Z.; Mazaheri, Y.; Rezagholizade-shirvan, A.; Mahmoudzadeh, M.; Sarafraz, M.; Mohtashami, M.; Shokri, S.; Ghasemi, A.; Nickfar, F.; Darroudi, M.; et al. The significance of essential oils and their antifungal properties in the food industry: A systematic review. *Heliyon* **2023**, *9*, e21386. [CrossRef]

27. da Rocha Neto, A.C.; Navarro, B.B.; Canton, L.; Maraschin, M.; Di Piero, R.M. Antifungal activity of palmarosa (*Cymbopogon martinii*), tea tree (*Melaleuca alternifolia*) and star anise (*Illicium verum*) essential oils against Penicillium expansum and their mechanisms of action. *LWT* **2019**, *105*, 385–392. [CrossRef]

28. Revathi, D.; Jaganathan, D.; Sivamani, P.; Arassu, R.R.T. Antifungal activity of palmarosa and geranuim, the natural essential oils against isolates from household refrigerators. *Int. J. Curr. Sci.* **2012**, *2012*, 58–66.

29. Carson, C.F.; Hammer, K.A.; Riley, T.V. Melaleuca alternifolia (Tea Tree) Oil: a Review of Antimicrobial and Other Medicinal Properties. *Clin. Microbiol. Rev.* **2006**, *19*, 50. [CrossRef]

30. Gemeda, N.; Tadele, A.; Lemma, H.; Girma, B.; Addis, G.; Tesfaye, B.; Abebe, A.; Gemechu, W.; Yirsaw, K.; Teka, F.; et al. Development,Characterization, and Evaluation of Novel Broad-Spectrum Antimicrobial Topical Formulations from Cymbopogon martini(Roxb.)W.Watson Essential Oil. *Evid.-Based Complement. Altern. Med.* **2018**, *2018*, 9812093. [CrossRef]

31. Simirgiotis, M.J.; Burton, D.; Parra, F.; López, J.; Muñoz, P.; Escobar, H.; Parra, C. Antioxidant and Antibacterial Capacities of Origanum vulgare L. Essential Oil from the Arid Andean Region of Chile and its Chemical Characterization by GC-MS. *Metabolites* **2020**, *10*, 414. [CrossRef]

32. Kim, S.; Lee, S.; Li, S. The Effect of Essential Oils from Tea-tree and Palmarosa on the Acne Skin. *Asian J. Beauty Cosmetol.* **2013**, *11*, 1083–1090.

33. Sinha, S.; Biswas, D.; Mukherjee, A. Antigenotoxic and antioxidant activities of palmarosa and citronella essential oils. *J. Ethnopharmacol.* **2011**, *137*, 1521–1527. [CrossRef] [PubMed]

34. Jesser, E.; Yeguerman, C.; Gili, V.; Santillan, G.; Murray, A.P.; Domini, C.; Werdin-González, J.O. Optimization and Characterization of Essential Oil Nanoemulsions Using Ultrasound for New Ecofriendly Insecticides. *Sustain. Chem. Eng.* **2020**, *8*, 7981–7992. [CrossRef]

35. Prashar, A.; Hili, P.; Veness, R.G.; Evans, C.S. Antimicrobial action of palmarosa oil (*Cymbopogon martinii*) on Saccharomyces cerevisiae. *Phytochemistry* **2003**, *63*, 569–575. [CrossRef]

36. Salvia-Trujillo, L.; Rojas-Graü, A.; Soliva-Fortuny, R.; Martín-Belloso, O. Physicochemical characterization and antimicrobial activity of food-grade emulsions and nanoemulsions incorporating essential oils. *Food Hydrocoll.* **2015**, *43*, 547–556. [CrossRef]

37. Wei, S.; Tian, Q.; Zhao, X.; Liu, X.; Husien, H.M.; Liu, M.; Li, J. Tea Tree Oil Nanoemulsion Potentiates Antibiotics against Multidrug-Resistant *Escherichia coli*. *ACS Infect. Dis.* **2022**, *8*, 1618–1626. [CrossRef]

38. Castro, J.C.; Pante, G.C.; de Souza, D.S.; Pires, T.Y.; Miyoshi, J.H.; Garcia, F.P.; Nakamura, C.V.; Mulati, A.C.N.; Mossini, S.A.G.; Junior, M.M.; et al. Molecular inclusion of Cymbopogon martinii essential oil with β−cyclodextrin as a strategy to stabilize and increase its bioactivity. *Food Hydrocoll. Health* **2022**, *2*, 100066. [CrossRef]

39. Lira, M.H.P.D.; de Andrade Júnior, F.P.; Moraes, G.F.Q.; da Silva Macena, G.; de Oliveira Pereira, F.; Lima, I.O. Antimicrobial activity of geraniol: an integrative review. *J. Essent. Oil Res.* **2020**, *32*, 187–197. [CrossRef]

40. Cox, S.D.; Mann, C.M.; Markham, J.L.; Gustafson, J.E.; Warmington, J.R.; Wyllie, S.G. Determining the Antimicrobial Actions of Tea Tree Oil. *Mol. J. Synth. Chem. Nat. Prod. Chem.* **2001**, *6*, 87. [CrossRef]

41. Maurya, A.; Singh, V.K.; Das, S.; Prasad, J.; Kedia, A.; Upadhyay, N.; Dubey, N.K.; Dwivedy, A.K. Essential Oil Nanoemulsion as Eco-Friendly and Safe Preservative: Bioefficacy Against Microbial Food Deterioration and Toxin Secretion, Mode of Action, and Future Opportunities. *Front. Microbiol.* **2021**, *12*, 751062. [CrossRef]

42. FDA Center for Drug Evaluation and Research. *Inactive Ingredient Search for Approved Drug Products*; U.S. Food & Drug Administration: Silver Spring, MD, USA, 2023.

43. Dávila-Rodríguez, M.; López-Malo, A.; Palou, E.; Ramírez-Corona, N.; Jiménez-Munguía, M.T. Essential oils microemulsions prepared with high-frequency ultrasound: physical properties and antimicrobial activity. *J. Food Sci. Technol.* **2020**, *57*, 4133–4142. [CrossRef] [PubMed]

44. Karunaratne, D.N.; Pamunuwa, G.; Ranatunga, U. Introductory Chapter: Microemulsions. In *Properties and Uses of Microemulsions*; Karunaratne, D.N., Pamunuwa, G., Ranatunga, U., Eds.; IntechOpen: Rijeka, Croatia, 2017; Chapter 1, pp. 2–12. [CrossRef]

45. Marinković, J.; Bošković, M.; Tasić, G.; Vasilijević, B.; Marković, D.; Marković, T.; Nikolić, B. Cymbopogon martinii essential oil nanoemulsions: Physico-chemical characterization, antibacterial and antibiofilm potential against Enterococcus faecalis. *Ind. Crops Prod.* **2022**, *187*, 115478. [CrossRef]

46. Falleh, H.; Jemaa, M.B.; Neves, M.A.; Isoda, H.; Nakajima, M.; Ksouri, R. Peppermint and Myrtle nanoemulsions: Formulation, stability, and antimicrobial activity. *LWT* **2021**, *152*, 112377. [CrossRef]

47. Nirmal, N.P.; Mereddy, R.; Li, L.; Sultanbawa, Y. Formulation, characterisation and antibacterial activity of lemon myrtle and anise myrtle essential oil in water nanoemulsion. *Food Chem.* **2018**, *254*, 1–7. [CrossRef]

48. Schulze, H. Schwefelarsen in wässriger Lösung. *J. Prakt. Chem.* **1882**, *25*, 431–452. [CrossRef]

49. Hardy, W.B.; Neville, F.H. A preliminary investigation of the conditions which determine the stability of irreversible hydrosols. *Proc. R. Soc. Lond.* **1900**, *66*, 110–125. [CrossRef]

50. Malvern Instruments Ltd. *Zetasizer Nano User Manual*; Malvern Instruments Ltd.: Malvern, UK, 2013.

51. Anarjan, N.; Tan, C.P. Developing a three component stabilizer system for producing astaxanthin nanodispersions. *Food Hydrocoll.* **2013**, *30*, 437–447. [CrossRef]

52. Patravale, V.B.; Date, A.A.; Kulkarni, R.M. Nanosuspensions: a promising drug delivery strategy. *J. Pharm. Pharmacol.* **2004**, *56*, 827–840. [CrossRef]

53. Gibis, M.; Rahn, N.; Weiss, J. Physical and Oxidative Stability of Uncoated and Chitosan-Coated Liposomes Containing Grape Seed Extract. *Pharmaceutics* **2013**, *5*, 421–433. [CrossRef]

54. Kahlweit, M.; Strey, R.; Busse, G. Microemulsions: a qualitative thermodynamic approach. *J. Phys. Chem.* **1990**, *94*, 3881–3894. [CrossRef]

55. Anton, N.; Vandamme, T. Nano-emulsions and Micro-emulsions: Clarifications of the Critical Differences. *Pharm. Res.* **2011**, *28*, 978–985. [CrossRef] [PubMed]

56. van Oss, C.J. Interfacial Phenomena in Apolar Media (Surfactant Science Series Vol. 21). H.F. Eicke and G.D. Parfitt, eds. Marcel Dekker, Inc., New York and Basel, 1987, pp ix + 416, $99.75. *J. Dispers. Sci. Technol.* **1990**, *11*, 435–436. [CrossRef]

57. Koroleva, Y.; Yurtovm, E. Nanoemulsions: the properties, methods of preparation and promising applications. *Russ. Chem. Rev.* **2012**, *81*, 21–43. [CrossRef]

58. Hategekimana, J.; Chamba, M.V.; Shoemaker, C.F.; Majeed, H.; Zhong, F. Vitamin E nanoemulsions by emulsion phase inversion: Effect of environmental stress and long-term storage on stability and degradation in different carrier oil types. *Colloids Surfaces Physicochem. Eng. Asp.* **2015**, *483*, 70–80. [CrossRef]

59. Erramreddy, V.V.; Tu, S.; Ghosh, S. Rheological reversibility and long-term stability of repulsive and attractive nanoemulsion gels. *RSC Adv.* **2017**, *7*, 47818–47832. [CrossRef]

60. Liu, L.; Niu, J.; Wu, J.Y. Development of highly stable paraffin wax/water phase change material nano-emulsions as potential coolants for thermal management. *Sol. Energy Mater. Sol. Cells* **2023**, *252*, 112184. [CrossRef]

61. Uluata, S.; McClements, D.J. Physical Stability, Autoxidation, and Photosensitized Oxidation of ω-3 Oils in Nanoemulsions Prepared with Natural and Synthetic Surfactants. *J. Agric. Food Chem.* **2015**, *63*, 933–9340. [CrossRef]

62. Hashemnejad, S.M.; Zarket, B.; Ricardo Castaneda, C.; Doyle, P.S. Thermoresponsive nanoemulsion-based gel synthesized through a low-energy process. *Nat. Commun.* **2019**, *10*, 2749. [CrossRef]

63. Silhavy, T.J.; Kahne, D.; Walker, S. The Bacterial Cell Envelope. *Cold Spring Harb. Perspect. Biol.* **2010**, *2*, 414. [CrossRef]

64. Hashem, A.H.; Doghish, A.S.; Ismail, A.; Hassanin, M.M.; Okla, M.K.; Saleh, I.A.; AbdElgawad, H.; Shehabeldine, A.M. A novel nanoemulsion based on clove and thyme essential oils: Characterization, antibacterial, antibiofilm and anticancer activities. *Electron. J. Biotechnol.* **2024**, *68*, 20–30. [CrossRef]

65. Linke, C.; Drusch, S. Turbidity in oil-in-water-emulsions — Key factors and visual perception. *Food Res. Int.* **2016**, *89*, 202–210. [CrossRef] [PubMed]

66. Čilek, A.; Čelebi, N.; Tirnaksiz, F. Lecithin-Based Microemulsion of a Peptide for Oral Administration: Preparation, Characterization, and Physical Stability of the Formulation. *Drug Deliv.* **2006**, *13*, 19–24. [CrossRef] [PubMed]

67. Aldrich Chemical Company. *Catalog Handbook of Fine Chemicals*; Aldrich Chemical Company: Milwaukee, WI, USA, 1990.

68. Berechet, M.D.; Chirilă, C.; Simion, D.; Niculescu, O.; Stanca, M.; Alexe, C.A.; Chelaru, C.; Râpă, M.; Gurău, D.F. Antifungal Activity of Leather Treated with Anethum graveolens and Melaleuca alternifolia Essential Oils against Trichophyton interdigitale. *Leather Footwear J.* **2020**, *20*, 133–144. [CrossRef]

69. Sanchez-Gaitan, E.; González-López, V.; Delgado, F. Characterization data FTIR and DLS for Palmarosa and Tea Tree nanoemulsions at 5% and 10%. *Mendeley Data* **2024**, *1*. [CrossRef]

70. Sarheed, O.; Dibi, M.; Ramesh, K.V.R.N.S. Studies on the Effect of Oil and Surfactant on the Formation of Alginate-Based O/W Lidocaine Nanocarriers Using Nanoemulsion Template. *Pharmaceutics* **2020**, *12*, 1223. [CrossRef]

71. Kepekçi, R.A.; İlçe, B.Y.; Kanmazalp, S.D. Plant-derived biomaterials for wound healing. In *Bioactive Natural Products*; ur Rahman, A., Ed.; Elsevier: Amsterdam, The Netherlands, 2021; Volume 70, pp. 227–264.

72. Gohel, M.; Soni, T.; Hingorani, L.; Patel, A.; Patel, N. Development and Optimization of Plant Extract Loaded Nanoemulsion Mixtures for the Treatment of Inflammatory Disorder. *Curr. Res. Drug Discov.* **2015**, *1*, 29–38. [CrossRef]

73. Maharini, I.; Utami, D.T.; Fitrianingsih. The Influence of Tween 80 in The Formulation of Nanoemulsion Virgin Coconut Oil. In *International Conference On Pharmaceutical Research And Practice 2018*; Universitas Islam Indonesia: Kota Depok, Indonesia, 2018; pp. 75–78.

74. Cortés, H.; Hernández-Parra, H.; Bernal-Chávez, S.A.; Prado-Audelo, M.L.D.; Caballero-Florán, I.H.; Borbolla-Jiménez, F.V.; González-Torres, M.; Magaña, J.J.; Leyva-Gómez, G. Non-Ionic Surfactants for Stabilization of Polymeric Nanoparticles for Biomedical Uses. *Materials* **2021**, *14*, 3197. [CrossRef]

75. Hunter, R.J. Influence of More Complex Adsorbates on Zeta Potential. In *Zeta Potential in Colloid Science*; Academic Press: Cambridge, MA, USA, 1981; pp. 305–344.

76. Bhatt, N.; Prasad, R.K.; Singh, K.; Panpalia, G.M. Stability study of O/W emulsions using zeta potential. *J. Chem. Pharm. Res.* **2010**, *2*, 512–527.

77. McClements, D.J. Nanoemulsions versus microemulsions: terminology, differences, and similarities. *Soft Matter* **2012**, *8*, 1719–1729. [CrossRef]

78. Fryd, M.M.; Mason, T.G. Time-Dependent Nanoemulsion Droplet Size Reduction By Evaporative Ripening. *Phys. Chem. Lett.* **2010**, *1*, 3349–3353. [CrossRef]

79. Park, J.; Kim, S.; Chang, Y.; Imm, J.Y. Synergistic antimicrobial effect and mode of action of palmarosa oil-loaded nanoemulsion and citric acid against Pectobacterium carotovorum. *Food Sci. Biotechnol.* **2023**, *32*, 823–831. [CrossRef] [PubMed]

80. Hombach, M.; Ochoa, C.; Maurer, F.P.; Pfiffner, T.; Böttger, E.C.; Furrer, R. Relative contribution of biological variation and technical variables to zone diameter variations of disc diffusion susceptibility testing. *J. Antimicrob. Chemother.* **2016**, *71*, 141–51. [CrossRef] [PubMed]

81. Doghish, A.S.; Shehabeldine, A.M.; El-Mahdy, H.A.; Hassanin, M.M.; Al-Askar, A.A.; Marey, S.A.; AbdElgawad, H.; Hashem, A.H. Thymus Vulgaris Oil Nanoemulsion: Synthesis, Characterization, Antimicrobial and Anticancer Activities. *Molecules* **2023**, *28*, 6910. [CrossRef] [PubMed]

82. da Silva, B.D.; do Rosário, D.K.A.; Neto, L.T.; Lelis, C.A.; Conte-Junior, C.A. Antioxidant, Antibacterial and Antibiofilm Activity of Nanoemulsion-Based Natural Compound Delivery Systems Compared with Non-Nanoemulsified Versions. *Foods* **2023**, *12*, 1901. [CrossRef] [PubMed]

83. Nazıroğlu, M.; Öznur D.; Öznur Ö.; Diler, A. In vitro antibacterial activity of Origanum onites and Mentha spicata subs tomentosa essential oil nanoemulsions against bacterial fish pathogens. *Acta Aquat. Turc.* **2022**, *18*, 495–504. [CrossRef]

84. Alkhatib, M.H.; Al-Husini, F.S.; Al-Amri, M.Y.; Al-Hatmi, A.; Al-Riyami, K.O.; Al-Ghafri, M.S. Antimicrobial Activity of Chitosan-vitamin E-Nanoemulsion. *J. Microbiol. Biotechnol. Food Sci.* **2023**, *13*, e10123. [CrossRef]

85. Kakaraparthi, P.S.; Srinivas, K.; Kumar, J.K.; Kumar, A.N.; Rajput, D.K.; Anubala, S. Changes in the essential oil content and composition of palmarosa (*Cymbopogon martini*) harvested at different stages and short intervals in two different seasons. *Ind. Crop. Prod.* **2015**, *69*, 348–354. [CrossRef]

86. Goddeeris, C.; Cuppo, F.; Reynaers, H.; Bouwman, W.; den Mooter, G.V. Light Scattering Measurements on Microemulsions: Estimation of Droplet Sizes. *Int. J. Pharm.* **2006**, *312*, 187–195. [CrossRef]

87. Thao Minh Ho, F.A.; Mikkonen, K.S. An overview of nanoemulsion characterization via atomic force microscopy. *Crit. Rev. Food Sci. Nutr.* **2022**, *62*, 4908–4928. [CrossRef] [PubMed]